JACS
JOURNAL OF THE AMERICAN CHEMICAL SOCIETY

Communication

pubs.acs.org/JACS

Structural Evolution of Atomically Precise Thiolated Bimetallic $[Au_{12+n}Cu_{32}(SR)_{30+n}]^{4-}$ (n = 0, 2, 4, 6) Nanoclusters

Huayan Yang,[†,§] Yu Wang,[†,§] Juanzhu Yan,[†] Xi Chen,[‡] Xin Zhang,[†] Hannu Häkkinen,[‡] and Nanfeng Zheng*[,†]

[†]State Key Laboratory for Physical Chemistry of Solid Surfaces, Collaborative Innovation Center of Chemistry for Energy Materials, and Department of Chemistry, College of Chemistry and Chemical Engineering, Xiamen University, Xiamen 361005, China

[‡]Departments of Physics and Chemistry, Nanoscience Center, University of Jyväskylä, FI-40014 Jyväskylä, Finland

Supporting Information

ABSTRACT: A series of all-thiol stabilized bimetallic Au−Cu nanoclusters, $[Au_{12+n}Cu_{32}(SR)_{30+n}]^{4-}$ (n = 0, 2, 4, 6 and SR = $SPhCF_3$), are successfully synthesized and characterized by X-ray single-crystal analysis and density functional theory (DFT) calculations. Each cluster consists of a Keplerate two-shell $Au_{12}@Cu_{20}$ core protected by $(6 - n)$ units of $Cu_2(SR)_5$ and n units of $Cu_2Au(SR)_6$ (n = 0, 2, 4, 6) motifs on its surface. The size and structural evolution of the clusters is atomically controlled by the Au precursors and countercations used in the syntheses. The clusters exhibit similar optical absorption properties that are not dependent on the number of surface $Cu_2Au(SR)_6$ units. Although DFT suggests an electronic structure with an 18-electron superatom shell closure, the clusters display different thermal stabilities. $[Au_{12+n}Cu_{32}(SR)_{30+n}]^{4-}$ clusters with n = 0 and 2 are more stable than those with n = 4 and 6. Moreover, an oxidation product of the clusters, $[Au_{13}Cu_{12}(SR)_{20}]^{4-}$, is structurally identified to gain insight into how the clusters are oxidized.

Bimetallic nanocrystals have attracted increasing research attention in recent years, mainly because of the complexity of their compositions and structures, which creates more opportunities to finely tune their physical and chemical properties.[1−5] Currently, high-quality bimetallic nanocrystals are mostly prepared by wet reduction chemistry assisted by the use of organic capping agents.[6,7] It has been well-documented that both the distribution of metals and the binding structure of capping ligands are vital to the overall properties of organic-capped bimetallic nanocrystals.[5] Nevertheless, until now there has been a lack of effective methods that allow the precise determination of molecular-level structures of bimetallic nanocrystals. Recently, an effective route has been developed to provide detailed molecular structures of metal nanoparticles by synthesizing and crystallizing organic-capped, atomic-precise metal nanoclusters into single crystals, followed by X-ray diffraction analysis.[8−18] This method has been extensively applied successfully to resolve the surface structure of thiol-capped Au nanoparticles.[8−14] Staple Au-thiol units (e.g., -RS-Au-SR-, -RS-Au-SR-Au-SR-) are revealed on the surface of all crystallographically determined thiol-capped Au nanoclusters and have become gradually accepted as a common surface structural feature for larger thiol-capped Au nanoparticles as well.[8−14] More recently, single-crystal analysis also demonstrated that both the core and surface structures of thiol-capped Ag nanoparticles could be significantly different from those of thiolated Au nanoparticles.[15−18] In the case of $[Au_{12}Ag_{32}(SR)_{30}]^{4-}$, Au and Ag were revealed to be distributed in a core−shell fashion rather than a random fashion, with all Ag atoms located on the surface of the clusters.[17] In the synthesis of $Au_{13}Cu_x$ clusters, the use of pyridyl-bearing ligands helped to control the number and location of Cu sites on the surface of icosahedral Au_{13} core and manipulate the catalytic exposure of Au atoms.[19]

In sharp contrast to the recent significant progress in identifying the molecular structures of thiolated Au and Ag nanoclusters, the synthesis and structure characterization of all-thiol capped metallic nanoclusters containing Cu have been rarely reported.[20,21] We now report our success in preparing a series of all-thiol capped bimetallic Au−Cu nanoclusters, $[Au_{12+n}Cu_{32}(SR)_{30+n}]^{4-}$ (n = 0, 2, 4, 6), and their crystal structures. Each $[Au_{12+n}Cu_{32}(SR)_{30+n}]^{4-}$ cluster is consisting of a Keplerate two-shell $Au_{12}@Cu_{20}$ core protected by $(6 - n)$ units of $Cu_2(SR)_5$ and n units of $Cu_2Au(SR)_6$ (n = 0, 2, 4, 6) on its surface. The metal distribution and the surface structure of the bimetallic nanoclusters were found to be highly sensitive to the Au precursors and countercations [i.e., tetraphenylphosphonium (PPh_4^+), tetrabutylammonium (NBu_4^+)] introduced in their syntheses. In the case of n = 2, 4, or 6, Au atoms are located at both the core and the surface of the clusters. The $[Au_{12+n}Cu_{32}(SR)_{30+n}]^{4-}$ clusters exhibited similar optical absorption properties. Density functional theory (DFT) calculations indicated an electronic structure with an 18-electron superatom shell closure in the metal core of the clusters and reproduced well the measured optical absorption spectra for clusters with n = 0, 2. The stability of the clusters was found to be highly dependent on their surface structures.

Synthesis of $[Au_{12+n}Cu_{32}(SR)_{30+n}]^{4-}$ nanoclusters involved the co-reduction of the Au(I) precursor [i.e., chloro(triphenylphosphine)gold(I) ($ClAuPPh_3$), chloro(diphenyl-2-pyridylphosphine)gold(I) (ClAuDPPy)] and $Cu(ClO_4)_2$ by aqueous $NaBH_4$ in the presence of 4-(trifluoromethyl)thiophenol and countercations. The synthesis was carried out in a mixed solvent of dichloromethane and methanol at 0 °C using an ice

Received: February 20, 2014
Published: May 5, 2014

   dx.doi.org/10.1021/ja501811j | J. Am. Chem. Soc. 2014, 136, 7197−7200

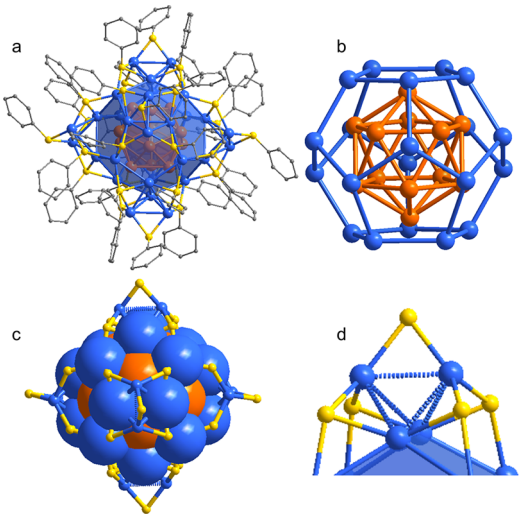

Figure 1. Crystal structure of the $[Au_{12}Cu_{32}(SR)_{30}]^{4-}$ cluster. (a) Overall structure of the $[Au_{12}Cu_{32}(SPhCF_3)_{30}]^{4-}$ cluster. All hydrogen and trifluoromethyl groups are omitted for clarity. (b) Two-shell $Au_{12}@Cu_{20}$ core of the cluster. (c) Structure of the cluster with the $Au_{12}@Cu_{20}$ two-shell cores in the space-filling style. (d) Structure of the surface $[Cu_2(SPhCF_3)_5]$ motif. Color legend: orange spheres, Au; blue spheres, Cu; yellow spheres, S; gray sticks/spheres, C.

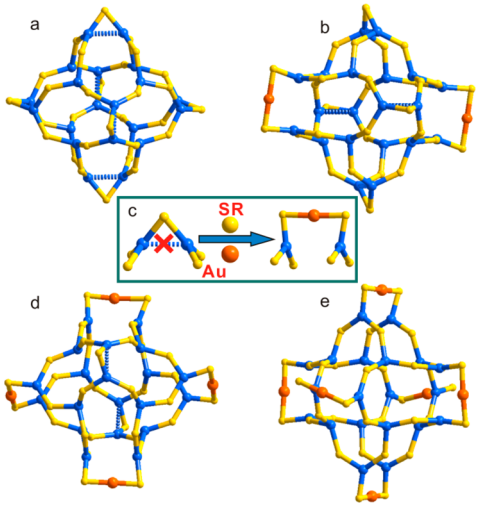

Figure 2. Surface structures of $Au_{12}Cu_{32}@Au_x$ (x = 0, 2, 4, 6) nanoclusters: (a) $[Au_{12}Cu_{32}(SR)_{30}]^{4-}$. (b) $[Au_{12}Cu_{32}Au_2(SR)_{32}]^{4-}$. (c) Schematic diagram of the formation of the $Cu_2Au(SR)_6$ unit from $Cu_2(SR)_5$ unit. (d) $[Au_{12}Cu_{32}Au_4(SR)_{34}]^{4-}$. (e) $[Au_{12}Cu_{32}Au_6(SR)_{36}]^{4-}$. Color legend: gold spheres, Au; blue spheres, Cu; yellow spheres, S. All hydrogen, fluorine, and carbon atoms are omitted for clarity.

bath (see Supporting Information for details). Crystallization of the nanoclusters was performed by layering hexane into the CH_2Cl_2 solution of clusters at 4 °C. The overall synthetic method was similar to that of $Au_{12}Ag_{32}$ clusters which we recently developed.[17] However, in the synthesis of Au−Cu bimetallic nanoclusters, the types of gold precursor and clusters' charge-balancing countercations were revealed to play important roles in determining the final structures of the bimetallic nanoclusters.

All the structures of $[Au_{12+n}Cu_{32}(SR)_{30+n}]^{4-}$ (n = 0, 2, 4, 6) clusters were determined by X-ray single crystal analysis (Table S1). When $ClAuPPh_3$ and PPh_4^+ were used as the gold precursor and the countercation, the obtained cluster was $Au_{12}Cu_{32}$ with n = 0. As illustrated in Figure 1a, $[Au_{12}Cu_{32}(SR)_{30}]^{4-}$ has a structure similar to $[Au_{12}Ag_{32}(SR)_{30}]^{4-}$.[17] The −4 charge of each cluster is balanced by four PPh_4^+ countercations (Figure S1). The core of the $Au_{12}Cu_{32}$ cluster can be depicted as an $Au_{12}@Cu_{20}$ Keplerate cage with a hollow Au_{12} icosahedron encapsulated in a pentagonal dodecahedral Cu_{20} shell (Figure 1b).

In the $[Au_{12}Cu_{32}(SR)_{30}]^{4-}$ cluster, each $Au_{12}@Cu_{20}$ Keplerate cage is further surface-capped by six $Cu_2(SR)_5$ units in an octahedral symmetry to form the final structure (Figure 1c). The $Cu_2(SR)_5$ unit can be better formulated as $(SR)_2$Cu-SR-Cu$(SR)_2$. Within the $Cu_2(SR)_5$ unit, each Cu atom is three-coordinated by three SR^- groups, sharing one bridging SR^- with the other Cu (Figure 1d). While the bridging SR^- does not bind to other Cu atoms, each of the other four thiolate groups in the $Cu_2(SR)_5$ unit further bind to two other Cu atoms on the dodecahedral Cu_{20} shell. Every two of the six $Cu_2(SR)_5$ units are equivalent, so they can be divided into three groups. The bridging angles of ∠Cu−SR−Cu are 76.1°, 75.2°, and 74.7°, respectively. The average Cu···Cu distance in six $Cu_2(SR)_5$ units is 2.763 Å (2.761−2.781 Å), 8% longer than the sum of Cu atomic radii (1.28 Å), indicating that there is no strong metal−metal interaction within the two Cu atoms of the $Cu_2(SR)_5$ units. In comparison, the surface Ag···Ag distance in $[Au_{12}Ag_{32}(SR)_{30}]^{4-}$ was averaged as 2.978 Å, only 3% longer than the sum of Ag atomic radii (1.44 Å).

To our surprise, the absence of a strong Cu···Cu interaction made the synthesis of $[Au_{12+n}Cu_{32}(SR)_{30+n}]^{4-}$ (n = 0, 2, 4, 6) highly sensitive to the synthetic conditions. Both the Au precursor and the countercation used in the synthesis were found critical in determining the final structure of the Au−Cu bimetallic nanoclusters (see Supporting Information for details). If $ClAuPPh_3$ was used and PPh_4Br was substituted by NBu_4Br, the synthesis led to the formation of $[Au_{14}Cu_{32}(SR)_{32}]^{4-}$ instead of $[Au_{12}Cu_{32}(SR)_{30}]^{4-}$. The $[Au_{14}Cu_{32}(SR)_{32}]^{4-}$cluster can be better formulated as $[Au_{12+n}Cu_{32}(SR)_{30+n}]^{4-}$ with n = 2. The $[Au_{12+2}Cu_{32}(SR)_{30+2}]^{4-}$cluster also contains a two-shell $Au_{12}@Cu_{20}$ Keplerate core (Figure S2). However, in contrast to $[Au_{12}Cu_{32}(SR)_{30}]^{4-}$ (Figure 2a), the $Au_{12}@Cu_{20}$ Keplerate core in $[Au_{12+2}Cu_{32}(SR)_{30+2}]^{4-}$ is capped by two pairs of $Cu_2(SR)_5$ units and one pair of $Cu_2Au(SR)_6$ units (Figure 2b), not three pairs of $Cu_2(SR)_5$ units. While the two Cu atoms in the $Cu_2(SR)_5$ unit are sharing a bridging thiolate, the two Cu atoms in the $Cu_2Au(SR)_6$ unit are connected by a linear $Au(SR)_2$ unit (Figure 2c). The surface $Cu_2Au(SR)_6$ unit can be thus structurally formulated as $(SR)_2$Cu-SR-Au-SR-Cu$(SR)_2$. The −4 charge in $[Au_{14}Cu_{32}(SR)_{32}]^{4-}$ clusters is well-balanced by four NBu_4^+ cations, as directly confirmed by the single-crystal analysis (see Table S1 for detailed crystal data).

More interestingly, if ClAuDPPy and PPh_4^+ were respectively used as the gold precursor and the countercation, the synthesis resulted in the formation of $[Au_{16}Cu_{32}(SR)_{34}]^{4-}$, another member of the series of $[Au_{12+n}Cu_{32}(SR)_{30+n}]^{4-}$ with n = 4 (Figure S3). As shown in Figure 2d, on the surface of $[Au_{16}Cu_{32}(SR)_{34}]^{4-}$, two pairs of $Cu_2Au(SR)_6$ units and one $Cu_2(SR)_5$ unit are capping the $Au_{12}@Cu_{20}$ core. Moreover, when the gold precursor was ClAuDPPy and the countercation was NBu_4^+, the synthesis yielded $[Au_{18}Cu_{32}(SR)_{36}]^{4-}$, namely $[Au_{12+n}Cu_{32}(SR)_{30+n}]^{4-}$ with n = 6 (Figure S4). In $[Au_{18}Cu_{32}(SR)_{36}]^{4-}$, the $Au_{12}@Cu_{20}$ core is protected by three pairs of

dx.doi.org/10.1021/ja501811j | J. Am. Chem. Soc. 2014, 136, 7197−7200

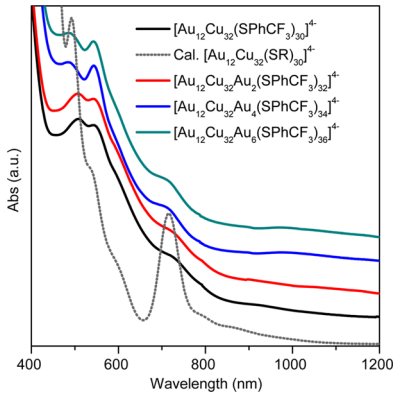

Figure 3. Optical absorption spectra of $[Au_{12}Cu_{32}(SPhCF_3)_{30}]\cdot 4PPh_4^+$, $[Au_{14}Cu_{32}(SPhCF_3)_{32}]\cdot 4NBu_4^+$, $[Au_{16}Cu_{32}(SPhCF_3)_{34}]\cdot 4PPh_4^+$, and $[Au_{18}Cu_{32}(SPhCF_3)_{36}]\cdot 4NBu_4^+$ in CH_2Cl_2 and the computed absorption spectrum for $[Au_{12}Cu_{32}(SR)_{30}]^{4-}$. In the theoretical spectrum, the individual optical transitions have been folded into a smooth curve by using a Gaussian width of 0.1 eV.

$Cu_2Au(SR)_6$ units (Figure 2e). These results suggested the important roles of reaction conditions, particularly the type of reactants, in determining the size and structural evolution of bimetallic nanoparticles.

Despite their different surface structures, the four $[Au_{12+n}Cu_{32}(SR)_{30+n}]^{4-}$ (n = 0, 2, 4, 6) clusters exhibited similar optical properties. As shown in Figure 3, the UV–vis–NIR absorption spectra of the four clusters in CH_2Cl_2 all displayed three obvious peaks at ~500, 543, and 711 nm, and one weak shoulder peaks at 600 nm. However, it should be pointed out that the peak at ~500 nm was slightly blue-shifted as more $Cu_2(SR)_5$ units were substituted by $Cu_2Au(SR)_6$. The electronic structures and optical properties of $[Au_{12+n}Cu_{32}(SR)_{30+n}]^{4-}$ clusters were studied via DFT computations (see Supporting Information for technical details). Structural details of the relaxed clusters are compared to the crystal structure data in Table S2. As shown previously for $[Ag_{44}(SR)_{30}]^{4-}$ and $[Au_{12}Ag_{32}(SR)_{30}]^{4-}$ clusters,[17] all these systems have a shell-closing number of 18 valence electrons in the metal core.[22] The calculated HOMO–LUMO energy gaps are 0.72, 0.72, 0.79, and 0.93 eV for n = 0, 2, 4, and 6, respectively. All clusters have the superatomic 1D states as highest occupied orbitals, and the manifold of the first few unoccupied orbitals shows the expected 1F and 2S symmetries (Figure S5).

The computed optical absorption spectrum of $[Au_{12}Cu_{32}(SR)_{30}]^{4-}$ (SR = SPh) is shown in Figure 3. It has two peaks at about 716 and 493 nm and two shoulders at about 600 and 542 nm. These features agree very well with the corresponding four features in the experimental spectrum, although the lowest-energy peak is more intense in the calculation. The computed spectrum of $[Au_{14}Cu_{32}(SR)_{32}]^{4-}$ is rather similar and is not shown here. We also analyzed the nature of the transitions at 716, 542, and 493 nm (details not shown here). This analysis showed that the lowest-energy peak is caused dominantly by the superatomic 1D → 1F transitions (Figure S6), while the higher-energy peaks have significant contributions from mixed metal–ligand transitions, where also the Au(5d) and Cu(3d) electrons contribute.

Although displaying little difference in their optical absorption properties, the four $[Au_{12+n}Cu_{32}(SR)_{30+n}]^{4-}$ (n = 0, 2, 4, 6) clusters have different stabilities. As Cu(0) is more prone to oxidation by air than Ag(0), $[Au_{12+n}Cu_{32}(SR)_{30+n}]^{4-}$ (n = 0, 2, 4, 6) clusters displayed much poorer stabilities than $[Au_{12}Ag_{32}(SR)_{30}]^{4-}$ clusters. At room temperature, when dissolved in solvents (i.e., DMF, CH_2Cl_2), only the $[Au_{12}Cu_{32}(SR)_{30}]^{4-}$ clusters were stable. The other three clusters were partly oxidized in solution after storage in air for 1 week. To better compare their stabilities, the single crystals of the clusters were dissolved in DMF and subjected to heat in air at 50 °C. UV–vis spectroscopy was applied to monitor the degradation of the clusters. The studies showed that all four clusters were degraded in DMF upon heating, with the intensities of all characteristic absorption peaks decreased with heating time (Figure S7). The peaks around 500 and 711 nm became broad gradually as the heating time was increased. After 2 h of heating, while all the other characteristic absorption peaks disappeared, the peak at 543 nm was still present. $[Au_{12}Cu_{32}(SR)_{30}]^{4-}$ and $[Au_{14}Cu_{32}(SR)_{32}]^{4-}$ exhibited better stabilities than $[Au_{16}Cu_{32}(SR)_{34}]^{4-}$ and $[Au_{18}Cu_{32}(SR)_{36}]^{4-}$. For $[Au_{12}Cu_{32}(SR)_{30}]^{4-}$ and $[Au_{14}Cu_{32}(SR)_{32}]^{4-}$, the peaks around 500 and 711 nm did not show obvious change in the first 10 min. For $[Au_{16}Cu_{32}(SR)_{34}]^{4-}$ and $[Au_{18}Cu_{32}(SR)_{36}]^{4-}$, the intensity of the peaks around 500 and 711 nm decreased significantly. The poorer stabilities of $[Au_{16}Cu_{32}(SR)_{34}]^{4-}$ and $[Au_{18}Cu_{32}(SR)_{36}]^{4-}$ might be explained by the presence of more $Cu_2Au(SR)_6$ units on their surfaces. The presence of more $Cu_2Au(SR)_6$ units would make the clusters more susceptible to oxidation by air. It should be noted that, in the absence of O_2, all $[Au_{12+n}Cu_{32}(SR)_{30+n}]^{4-}$ (n = 0, 2, 4, 6) clusters are stable at room temperature. No obvious change in the optical absorptions of their solutions in CH_2Cl_2 was observed in 6 days (Figure S8).

To understand the degradation process of the $[Au_{12+n}Cu_{32}(SR)_{30+n}]^{4-}$ clusters, much effort was made to crystallize the degradation products by dissolving them in CH_2Cl_2 and diffusing the solution with hexane. We were fortunate to obtain single crystals of the degradation products of $[Au_{16}Cu_{32}(SR)_{34}]^{4-}$ clusters. X-ray single-crystal analysis revealed the cocrystallization of $[Au_{13}Cu_{12}(SPhCF_3)_{20}]^{4-}$ clusters with PPh_4^+ as countercations in the obtained single crystals (Figure S9). In contrast to its parent $[Au_{16}Cu_{32}(SR)_{34}]^{4-}$ cluster, each $[Au_{13}Cu_{12}(SPhCF_3)_{20}]^{4-}$ cluster has a solid icosahedral Au_{13} unit instead of a hollow Au_{12} unit as its core (Figure 4a). The icosahedral Au_{12} shell is protected by two $Cu_6(SR)_{10}$ units at centrosymmetric positions with respect to the central Au of the Au_{13} unit (Figure 4b). Structurally, the icosahedral Au_{12} shell consists of two jointed C_3-symmetric Au_6 units, each of which is capped by a $Cu_6(SR)_{10}$ unit. The arrangement of the six Cu atoms in $Cu_6(SR)_{10}$ resembles that of a C_3-symmetric Au_6 unit on the icosahedral Au_{12} shell (Figure 4c). However, the 12 Cu atoms from the two $Cu_6(SR)_{10}$ units are not enough to yield a close shell on the Au_{13} core, due to the longer distance between Cu and the central Au atom. The two $Cu_6(SR)_{10}$ units are separated from each other. In each $Cu_6(SR)_{10}$ unit, one thiolate is face-capping the center Cu_3 unit as a μ_3 ligand. The other nine thiolate groups are equally divided into three different types (Figure 4c). Both μ_2 and μ_3 thiolate ligands, each bound to only one Au, are identified between the Au_{12} shell and the Cu shell. Each of the other three thiolate ligands serves as a μ_2 ligand to joint two Cu outward at the edge of the $Cu_6(SR)_{10}$ unit. As a result, all Cu atoms in the $[Au_{13}Cu_{12}(SPhCF_3)_{20}]^{4-}$ cluster are planar-coordinated by three thiolates, similar to that observed in $Au_{13}Cu_x$ clusters. This situation makes the surface

dx.doi.org/10.1021/ja501811j | J. Am. Chem. Soc. 2014, 136, 7197–7200

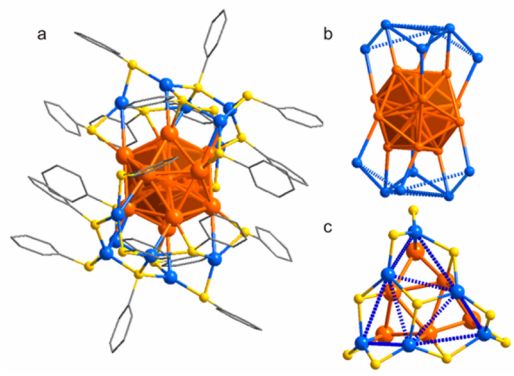

Figure 4. Crystal structure of the $[Au_{13}Cu_{12}(SPhCF_3)_{20}]^{4-}$ cluster. (a) Overall structure of the cluster. (b) Side view of the capping of two $Cu_6(SR)_{10}$ units on the Au_{13} core. (c) Top view showing how $Cu_2Au(SR)_6$ is sitting on the Au_6 unit of the Au_{12} shell. Color legend: gold spheres, Au; blue spheres, Cu; yellow spheres, S. All hydrogen atoms and trifluoromethyl groups in (a) and fluorine and carbon atoms in (b) and (c) are omitted for clarity.

structure of the $[Au_{13}Cu_{12}(SPhCF_3)_{20}]^{4-}$ cluster totally different from that of the $Au_{25}(SR)_{18}$ cluster, in which the Au_{13} core is evenly capped by six -RS-Au-SR-Au-SR- units although both clusters contain the same number of metal atoms. Successful structural determination of the degradation product of the $[Au_{12+n}Cu_{32}(SR)_{30+n}]^{4-}$ clusters suggested that their instability in solution was mainly due to the easy oxidation of low-valent Cu by air. To our surprise, even with a nine-electron structure, the oxidation product, $[Au_{13}Cu_{12}(SPhCF_3)_{20}]^{4-}$, was much more stable than its parent $[Au_{16}Cu_{32}(SR)_{34}]^{4-}$ cluster. The $[Au_{13}Cu_{12}(SPhCF_3)_{20}]^{4-}$ cluster exhibited a major absorption at 540 nm (Figure S10). No obvious decay was observed, even after its DMF solution was heated in air at 80 °C for 1.5 h.

To summarize, a series of all-thiol capped bimetallic Au−Cu nanoclusters, $[Au_{12+n}Cu_{32}(SR)_{30+n}]^{4-}$ (n = 0, 2, 4, 6), have been successfully prepared. The metal distribution and the surface structure of the bimetallic nanoclusters were found to be highly sensitive to the Au precursors and countercations used in the syntheses. Each $[Au_{12+n}Cu_{32}(SR)_{30+n}]^{4-}$ (n = 0, 2, 4, 6) cluster consists of a Keplerate two-shell $Au_{12}@Cu_{20}$ core protected by $(6 - n)$ units of $Cu_2(SR)_5$ and n units of $Cu_2Au(SR)_6$ (n = 0, 2, 4, 6) on its surface. Different surface structures among the clusters did not result in obvious differences in their absorption properties but did lead to different stabilities. $[Au_{12}Cu_{32}(SR)_{30}]^{4-}$ and $[Au_{14}Cu_{32}(SR)_{32}]^{4-}$ exhibited better stabilities than $[Au_{16}Cu_{32}(SR)_{34}]^{4-}$ and $[Au_{18}Cu_{32}(SR)_{36}]^{4-}$. Structural determination of the degradation product of the $[Au_{12+n}Cu_{32}(SR)_{30+n}]^{4-}$ clusters clearly indicated that the poor stability of thiolated Au−Cu bimetallic nanoclusters was mainly due to the easy oxidation of zerovalent Cu by air.

■ ASSOCIATED CONTENT

Supporting Information

Experimental details, detailed crystallographic data including the CIF files, computational details, UV−vis spectra of $[Au_{12+n}Cu_{32}(SPhCF_3)_{30+n}]^{4-}$ (n = 0, 2, 4, 6) clusters, UV−vis spectra of $[Au_{13}Cu_{12}(SPhCF_3)_{20}]\cdot 4PPh_4^+$, comparison of computed and experimental bond lengths, analysis of the electronic structure, and optical transitions of $[Au_{12}Cu_{32}(SR)_{30}]^{4-}$. This material is available free of charge via the Internet at http://pubs.acs.org.

■ AUTHOR INFORMATION

Corresponding Author

nfzheng@xmu.edu.cn

Author Contributions

§H.Y. and Y.W. contributed equally to this work.

Notes

The authors declare no competing financial interest.

■ ACKNOWLEDGMENTS

We thank the MOST of China (2011CB932403) and the NSFC of China (21131005, 21390390, 21333008) for financial support. The work in University of Jyväskylä was supported by the Academy of Finland. The computations were made at the CSC computing center in Espoo, Finland, and at the HLRS center in Stuttgart, Germany. X.C. thanks L. Lehtovaara for discussions on DFT analysis of optical spectra.

■ REFERENCES

(1) Ferrando, R.; Jellinek, J.; Johnston, R. L. *Chem. Rev.* **2008**, *108*, 845.
(2) Wang, D.; Li, Y. *Adv. Mater.* **2011**, *23*, 1044.
(3) Pan, C.; Dassenoy, F.; Casanove, M.-J.; Philippot, K.; Amiens, C.; Lecante, P.; Mosset, A.; Chaudret, B. *J. Phys. Chem. B* **1999**, *103*, 10098.
(4) Zhang, Y.; Huang, W.; Habas, S. E.; Kuhn, J. N.; Grass, M. E.; Yamada, Y.; Yang, P.; Somorjai, G. A. *J. Phys. Chem. C* **2008**, *112*, 12092.
(5) Hong, J.-W.; Kim, D.-H.; Lee, Y.-W.; Kim, M.-J.; Kang, S.-W.; Han, S.-W. *Angew. Chem., Int. Ed.* **2011**, *50*, 8876.
(6) Wu, B. H.; Zheng, N. F. *Nano Today* **2013**, *8*, 168.
(7) Niu, Z.; Li, Y. *Chem. Mater.* **2013**, *26*, 72.
(8) Zeng, C.; Qian, H.; Li, T.; Li, G.; Rosi, N. L.; Yoon, B.; Barnett, R. N.; Whetten, R. L.; Landman, U.; Jin, R. *Angew. Chem.* **2012**, *124*, 13291.
(9) Heaven, M. W.; Dass, A.; White, P. S.; Holt, K. M.; Murray, R. W. *J. Am. Chem. Soc.* **2008**, *130*, 3754.
(10) Das, A.; Li, T.; Nobusada, K.; Zeng, C.; Rosi, N. L.; Jin, R. *J. Am. Chem. Soc.* **2013**, *135*, 18264.
(11) Das, A.; Li, T.; Nobusada, K.; Zeng, Q.; Rosi, N. L.; Jin, R. *J. Am. Chem. Soc.* **2012**, *134*, 20286.
(12) Qian, H. F.; Eckenhoff, W. T.; Zhu, Y.; Pintauer, T.; Jin, R. C. *J. Am. Chem. Soc.* **2010**, *132*, 8280.
(13) Zeng, C. J.; Li, T.; Das, A.; Rosi, N. L.; Jin, R. C. *J. Am. Chem. Soc.* **2013**, *135*, 10011.
(14) Jadzinsky, P. D.; Calero, G.; Ackerson, C. J.; Bushnell, D. A.; Kornberg, R. D. *Science* **2007**, *318*, 430.
(15) Yang, H. Y.; Lei, J.; Wu, B. H.; Wang, Y.; Zhou, M.; Xia, A. D.; Zheng, L. S.; Zheng, N. F. *Chem. Commun.* **2013**, *49*, 300.
(16) Yang, H. Y.; Wang, Y.; Zheng, N. F. *Nanoscale* **2013**, *5*, 2674.
(17) Yang, H. Y.; Wang, Y.; Huang, H. Q.; Gell, L.; Lehtovaara, L.; Malola, S.; Häkkinen, H.; Zheng, N. F. *Nat. Commun.* **2013**, *4*, 2422.
(18) Desireddy, A.; Conn, B. E.; Guo, J.; Yoon, B.; Barnett, R. N.; Monahan, B. M.; Kirschbaum, K.; Griffith, W. P.; Whetten, R. L.; Landman, U.; Bigioni, T. P. *Nature* **2013**, *501*, 399.
(19) Yang, H.; Wang, Y.; Lei, J.; Shi, L.; Wu, X.; Mäkinen, V.; Lin, S.; Tang, Z.; He, J.; Häkkinen, H.; Zheng, L.; Zheng, N. *J. Am. Chem. Soc.* **2013**, *135*, 9568.
(20) Negishi, Y.; Munakata, K.; Ohgake, W.; Nobusada, K. *J. Phys. Chem. Lett.* **2012**, *3*, 2209.
(21) Dhayal, R. S.; Liao, J.-H.; Lin, Y.-R.; Liao, P.-K.; Kahlal, S.; Saillard, J.-Y.; Liu, C. W. *J. Am. Chem. Soc.* **2013**, *135*, 4704.
(22) Walter, M.; Akola, J.; Lopez-Acevedo, O.; Jadzinsky, P. D.; Calero, G.; Ackerson, C. J.; Whetten, R. L.; Gronbeck, H.; Häkkinen, H. *Proc. Natl. Acad. Sci. U.S.A.* **2008**, *105*, 9157.